The Journal of Chemical Physics

RESEARCH ARTICLE | MAY 08 2024

Current density functional framework for spin–orbit coupling: Extension to periodic systems

Yannick J. Franzke ; Christof Holzer

J. Chem. Phys. 160, 184101 (2024)
https://doi.org/10.1063/5.0209704

AIP Publishing

The Journal of Chemical Physics ARTICLE pubs.aip.org/aip/jcp

Current density functional framework for spin–orbit coupling: Extension to periodic systems

Cite as: J. Chem. Phys. 160, 184101 (2024); doi: 10.1063/5.0209704
Submitted: 22 March 2024 • Accepted: 20 April 2024 •
Published Online: 8 May 2024

Yannick J. Franzke[1,a] and Christof Holzer[2,a]

AFFILIATIONS

[1] Otto Schott Institute of Materials Research, Friedrich Schiller University Jena, Löbdergraben 32, 07743 Jena, Germany
[2] Institute of Theoretical Solid State Physics, Karlsruhe Institute of Technology (KIT), Wolfgang-Gaede-Straße 1, 76131 Karlsruhe, Germany

[a] **Authors to whom correspondence should be addressed:** christof.holzer@kit.edu and yannick.franzke@uni-jena.de

ABSTRACT

Spin–orbit coupling induces a current density in the ground state, which consequently requires a generalization for *meta*-generalized gradient approximations. That is, the exchange–correlation energy has to be constructed as an explicit functional of the current density, and a generalized kinetic energy density has to be formed to satisfy theoretical constraints. Herein, we generalize our previously presented formalism of spin–orbit current density functional theory [Holzer *et al.*, J. Chem. Phys. **157**, 204102 (2022)] to non-magnetic and magnetic periodic systems of arbitrary dimension. In addition to the ground-state exchange–correlation potential, analytical derivatives such as geometry gradients and stress tensors are implemented. The importance of the current density is assessed for band gaps, lattice constants, magnetic transitions, and Rashba splittings. In the latter, the impact of the current density may be larger than the deviation between different density functional approximations.

I. INTRODUCTION

In the constantly evolving field of density functional theory (DFT), especially the construction of *meta*-generalized gradient approximations (meta-GGAs) has received great attention over the last two decades.[1–4] Modern meta-GGAs use the iso-orbital constraint and the von Weizäcker inequality to identify one-electron regions, thus canceling self-interaction errors in single electron regions.[3,5] According to benchmark calculations,[4,6–21] meta-GGAs outperform the preceding generalized gradient approximations (GGAs) at roughly the same computational cost. However, external magnetic fields[22–25] or spin–orbit coupling[26–28] necessitate further generalizations for meta-GGAs to meet theoretical constraints, as the current density alters the curvature of the Fermi hole in its second-order Taylor expansion.[29–38] Density functional approximations (DFAs) constructed by taking into account this change in curvature are termed current-dependent DFT (CDFT) functionals.[22,39] CDFT based approximations are, for example, necessary for the iso-orbital indicator to remain bounded between 0 and 1.[35,36] In external magnetic fields, this correction is even necessary to guarantee gauge-invariance.[22,25,36]

Furthermore, certain current-carrying ground states also heavily depend on the correct introduction of the current density, with a failure to account for them leading to a large deviation for meta-GGAs.[36,40] We recently presented a current-dependent formulation of density functional theory for spin–orbit coupling in the molecular regime.[36] Here, the inclusion of the current density leads to notable changes for both closed-shell Kramers-restricted (KR) and open-shell Kramers-unrestricted (KU) calculations.

To account for the change in Fermi hole curvature, the kinetic energy density τ is generalized with the current density $\vec{j}$. In a two-component (2c) non-collinear formalism,[41–51] this results in the generalized current density,

$$\tilde{\tau}_{\uparrow,\downarrow} = \tau_{\uparrow,\downarrow} - \frac{|\vec{j}_{\uparrow,\downarrow}|^2}{2n_{\uparrow,\downarrow}}, \tag{1}$$

based on the spin-up and spin-down quantities.[36] These are formed with the particle and spin-magnetization contributions, e.g., the spin-up and spin-down electron density $n_{\uparrow,\downarrow}$, which follows as

$$n_{\uparrow,\downarrow}(\vec{r}) = \frac{1}{2}\left[n(\vec{r}) \pm |\vec{m}(\vec{r})|\right] = \frac{1}{2}\left[n(\vec{r}) \pm s(\vec{r})\right], \tag{2}$$

with the particle density n, the spin-magnetization vector $\vec{m}$, and the spin density s. Therefore, the exchange–correlation (XC) energy of a "pure" functional[2] explicitly depends on the current density,

$$\begin{aligned} E^{\mathrm{XC}} &= \int f^{\mathrm{XC}}\left[n_{\uparrow,\downarrow}(\vec{r}), \gamma_{\uparrow\uparrow,\uparrow\downarrow,\downarrow\downarrow}(\vec{r}), \tau_{\uparrow,\downarrow}(\vec{r}), \vec{j}_{\uparrow,\downarrow}(\vec{r})\right] \mathrm{d}^3 r \\ &= \int g^{\mathrm{XC}}\left[n_{\uparrow,\downarrow}(\vec{r}), \gamma_{\uparrow\uparrow,\uparrow\downarrow,\downarrow\downarrow}(\vec{r}), \tilde{\tau}_{\uparrow,\downarrow}(\vec{r})\right] \mathrm{d}^3 r, \end{aligned} \tag{3}$$

where f^{XC} describes the density functional approximation and $\gamma_{\uparrow\downarrow}(\vec{r}) = \frac{1}{4}\left(\vec{\nabla} n_{\uparrow}(\vec{r})\right) \cdot \left(\vec{\nabla} n_{\downarrow}(\vec{r})\right)$, hence $\gamma_{\uparrow\downarrow} = \gamma_{\downarrow\uparrow}$. For a Kramers-restricted system, the spin-magnetization vector and the particle current density vanish. However, the spin-current density is generally non-zero, and thus, it is still necessary to form the generalized kinetic energy density.

In this work, we will extend our previous CDFT formulation[36] to non-magnetic and magnetic periodic systems. We assess the importance of the current density for band gaps, cell structures, magnetic transitions, and Rashba splittings with common meta-GGAs. Together with previous studies on the impact of spin–orbit-induced current densities for meta-GGAs,[36,38,52–54] this will further help to set guidelines and recommendations for the application of CDFT to the different properties and functionals of discrete and periodic systems.

II. THEORY

The one-particle density matrix associated with the two-component spinor functions $\vec{\psi}_i^{\vec{k}}$ at a given $\vec{k}$ point reads

$$\begin{aligned} n(\vec{r},\vec{r}\,') &= \frac{1}{V_{\mathrm{FBZ}}} \sum_{i=1}^{n} \int_{\mathrm{FBZ}}^{\varepsilon_i^{\vec{k}} < \varepsilon_{\mathrm{F}}} \vec{\psi}_i^{\vec{k}}(\vec{r}) \left(\vec{\psi}_i^{\vec{k}}(\vec{r}\,')\right)^{\dagger} \mathrm{d}^3 k \\ &= \begin{pmatrix} n^{\alpha\alpha}(\vec{r},\vec{r}\,') & n^{\alpha\beta}(\vec{r},\vec{r}\,') \\ n^{\beta\alpha}(\vec{r},\vec{r}\,') & n^{\beta\beta}(\vec{r},\vec{r}\,') \end{pmatrix}, \end{aligned} \tag{4}$$

where V_{FBZ} is the volume of the first Brillouin zone (FBZ), ε_i is the energy eigenvalue, and ε_{F} is the Fermi level. The spinor functions are expanded with Bloch functions, ϕ_μ, based on atomic orbital (AO) basis functions, χ_μ, as

$$\vec{\psi}_i^{\vec{k}}(\vec{r}) = \begin{pmatrix} \psi_i^{\alpha,\vec{k}}(\vec{r}) \\ \psi_i^{\beta,\vec{k}}(\vec{r}) \end{pmatrix} = \sum_{\mu} \begin{pmatrix} c_{\mu i}^{\alpha,\vec{k}} \\ c_{\mu i}^{\beta,\vec{k}} \end{pmatrix} \phi_\mu^{\vec{k}}(\vec{r}), \tag{5}$$

$$\phi_\mu^{\vec{k}}(\vec{r}) = \frac{1}{\sqrt{N_{\mathrm{UC}}}} \sum_{\vec{L}} e^{\mathrm{i}\vec{k}\cdot\vec{L}}\, \chi_\mu^{\vec{L}}(\vec{r}). \tag{6}$$

N_{UC} denotes the number of electrons in the unit cell (UC) and $\vec{L}$ denotes the lattice vector. Thus, all density variables are available from the AO density matrix in the position space given by

$$D_{\mu\nu}^{\sigma\sigma',\vec{L}\vec{L}\,'} = \frac{1}{V_{\mathrm{FBZ}}} \sum_i \int_{\mathrm{FBZ}}^{\varepsilon_i^{\vec{k}} < \varepsilon_{\mathrm{F}}} e^{\mathrm{i}\vec{k}\cdot\left[\vec{L}-\vec{L}\,'\right]} \left(c_{\mu i}^{\sigma,\vec{k}}\; c_{\nu i}^{*\sigma',\vec{k}}\right) \mathrm{d}^3 k, \tag{7}$$

with the expansion coefficients $c_{\mu i}$ and $\sigma, \sigma' \in \{\alpha, \beta\}$. The complete two-component AO density matrix reads

$$\mathbf{D}^{\vec{L}\vec{L}\,'} = \begin{pmatrix} \mathbf{D}^{\alpha\alpha} & \mathbf{D}^{\alpha\beta} \\ \mathbf{D}^{\beta\alpha} & \mathbf{D}^{\beta\beta} \end{pmatrix}^{\vec{L}\vec{L}\,'} \quad \text{with} \quad \left(\mathbf{D}^{\vec{L}\vec{L}\,'}\right)^{\dagger} = \mathbf{D}^{\vec{L}\,'\vec{L}}. \tag{8}$$

In the spirit of Bulik *et al.*,[47] the real symmetric (RS), real antisymmetric (RA), imaginary symmetric (IS), and imaginary antisymmetric (OA) linear combinations,

$$\left[\mathbf{D}_{\mathrm{RS,\,RA}}^{\sigma\sigma'}\right]^{\vec{L}\vec{L}\,'} = \frac{1}{2}\left[\mathrm{Re}\left(\mathbf{D}^{\sigma\sigma'} \pm \mathbf{D}^{\sigma'\sigma}\right)\right]^{\vec{L}\vec{L}\,'}, \tag{9}$$

$$\left[\mathbf{D}_{\mathrm{IA,\,IS}}^{\sigma\sigma'}\right]^{\vec{L}\vec{L}\,'} = \frac{1}{2}\left[\mathrm{Im}\left(\mathbf{D}^{\sigma\sigma'} \pm \mathbf{D}^{\sigma'\sigma}\right)\right]^{\vec{L}\vec{L}\,'}, \tag{10}$$

are formed. Of course, the same-spin antisymmetric contributions are zero. The electron density and its derivatives are available for symmetric linear combinations,

$$n(\vec{r}) = \sum_{\mu\nu} \sum_{\vec{L}\vec{L}\,'} \left[\mathbf{D}_{\mathrm{RS}}^{\alpha\alpha} + \mathbf{D}_{\mathrm{RS}}^{\beta\beta}\right]_{\mu\nu}^{\vec{L}\vec{L}\,'} \chi_\mu^{\vec{L}}(\vec{r})\, \chi_\nu^{\vec{L}\,'}(\vec{r}), \tag{11}$$

$$m_x(\vec{r}) = \sum_{\mu\nu} \sum_{\vec{L}\vec{L}\,'} 2\left[\mathbf{D}_{\mathrm{RS}}^{\alpha\beta}\right]_{\mu\nu}^{\vec{L}\vec{L}\,'} \chi_\mu^{\vec{L}}(\vec{r})\, \chi_\nu^{\vec{L}\,'}(\vec{r}), \tag{12}$$

$$m_y(\vec{r}) = \sum_{\mu\nu} \sum_{\vec{L}\vec{L}\,'} 2\left[\mathbf{D}_{\mathrm{IS}}^{\alpha\beta}\right]_{\mu\nu}^{\vec{L}\vec{L}\,'} \chi_\mu^{\vec{L}}(\vec{r})\, \chi_\nu^{\vec{L}\,'}(\vec{r}), \tag{13}$$

$$m_z(\vec{r}) = \sum_{\mu\nu} \sum_{\vec{L}\vec{L}\,'} \left[\mathbf{D}_{\mathrm{RS}}^{\alpha\alpha} - \mathbf{D}_{\mathrm{RS}}^{\beta\beta}\right]_{\mu\nu}^{\vec{L}\vec{L}\,'} \chi_\mu^{\vec{L}}(\vec{r})\, \chi_\nu^{\vec{L}\,'}(\vec{r}). \tag{14}$$

The particle current density $\vec{j}_{\mathrm{p}}$ and the spin-current densities $\vec{j}_u$, with $u \in \{x, y, z\}$, are obtained from the antisymmetric linear combinations,

$$\vec{j}_{\mathrm{p}}(\vec{r}) = -\frac{\mathrm{i}}{2} \sum_{\mu\nu} \sum_{\vec{L}\vec{L}\,'} \left[\mathbf{D}_{\mathrm{IA}}^{\alpha\alpha} + \mathbf{D}_{\mathrm{IA}}^{\beta\beta}\right]_{\mu\nu}^{\vec{L}\vec{L}\,'} \xi_{\mu\nu}^{\vec{L}\vec{L}\,'}, \tag{15}$$

$$\vec{j}_x(\vec{r}) = -\frac{\mathrm{i}}{2} \sum_{\mu\nu} \sum_{\vec{L}\vec{L}\,'} 2\left[\mathbf{D}_{\mathrm{IA}}^{\alpha\beta}\right]_{\mu\nu}^{\vec{L}\vec{L}\,'} \xi_{\mu\nu}^{\vec{L}\vec{L}\,'}, \tag{16}$$

$$\vec{j}_y(\vec{r}) = -\frac{\mathrm{i}}{2} \sum_{\mu\nu} \sum_{\vec{L}\vec{L}\,'} 2\left[\mathbf{D}_{\mathrm{RA}}^{\alpha\beta}\right]_{\mu\nu}^{\vec{L}\vec{L}\,'} \xi_{\mu\nu}^{\vec{L}\vec{L}\,'}, \tag{17}$$

$$\vec{j}_z(\vec{r}) = -\frac{\mathrm{i}}{2} \sum_{\mu\nu} \sum_{\vec{L}\vec{L}\,'} \left[\mathbf{D}_{\mathrm{IA}}^{\alpha\alpha} - \mathbf{D}_{\mathrm{IA}}^{\beta\beta}\right]_{\mu\nu}^{\vec{L}\vec{L}\,'} \xi_{\mu\nu}^{\vec{L}\vec{L}\,'}, \tag{18}$$

with

$$\xi_{\mu\nu}^{\vec{L}\vec{L}\,'} = \left\{\left[\vec{\nabla}\chi_\mu^{\vec{L}}(\vec{r})\right] \chi_\nu^{\vec{L}\,'}(\vec{r}) - \chi_\mu^{\vec{L}}(\vec{r}) \left[\vec{\nabla}\chi_\nu^{\vec{L}\,'}(\vec{r})\right]\right\}. \tag{19}$$

Following our molecular ansatz,[36] the scalar part of the XC potential is obtained as

$$
\begin{aligned}
V^{\mathrm{XC},\vec{L}\vec{L}'}_{\mu\nu,0} = {} & \frac{1}{2}\int\left[\frac{\partial g^{\mathrm{XC}}}{\partial n_\uparrow}+\frac{\partial g^{\mathrm{XC}}}{\partial n_\downarrow}\right]\chi^{\vec{L}}_\mu(\vec{r})\,\chi^{\vec{L}'}_\nu(\vec{r})\,\mathrm{d}^3r \\
& + \frac{1}{2}\int\left[\frac{|\vec{j}_\uparrow|^2}{2n_\uparrow^2}\frac{\partial g^{\mathrm{XC}}}{\partial n_\downarrow}+\frac{|\vec{j}_\downarrow|^2}{2n_\downarrow^2}\frac{\partial g^{\mathrm{XC}}}{\partial \tilde{\tau}_\downarrow}\right]\chi^{\vec{L}}_\mu(\vec{r})\,\chi^{\vec{L}'}_\nu(\vec{r})\,\mathrm{d}^3r \\
& - \frac{1}{2}\int\left[2\frac{\partial g^{\mathrm{XC}}}{\partial \gamma_{\uparrow\uparrow}}\vec{\nabla}n_\uparrow + 2\frac{\partial g^{\mathrm{XC}}}{\partial \gamma_{\downarrow\downarrow}}\vec{\nabla}n_\downarrow + \frac{\partial g^{\mathrm{XC}}}{\partial \gamma_{\uparrow\downarrow}}(\vec{\nabla}n_\uparrow+\vec{\nabla}n_\downarrow)\right] \\
& \times\left[\left\{\vec{\nabla}\chi^{\vec{L}}_\mu(\vec{r})\right\}\chi^{\vec{L}'}_\nu(\vec{r}) + \chi^{\vec{L}}_\mu(\vec{r})\left\{\vec{\nabla}\chi^{\vec{L}'}_\nu(\vec{r})\right\}\right]\mathrm{d}^3r \\
& + \int\frac{1}{2}\left[\frac{\partial g^{\mathrm{XC}}}{\partial \tilde{\tau}_\uparrow}+\frac{\partial g^{\mathrm{XC}}}{\partial \tilde{\tau}_\downarrow}\right]\left[\vec{\nabla}\chi^{\vec{L}}_\mu(\vec{r})\right]\cdot\left[\vec{\nabla}\chi^{\vec{L}'}_\nu(\vec{r})\right]\mathrm{d}^3r \\
& + \int\frac{\mathrm{i}}{2}\left[\frac{\vec{j}_\uparrow}{n_\uparrow}\frac{\partial g^{\mathrm{XC}}}{\partial \tilde{\tau}_\uparrow}+\frac{\vec{j}_\downarrow}{n_\downarrow}\frac{\partial g^{\mathrm{XC}}}{\partial \tilde{\tau}_\downarrow}\right]\xi^{\vec{L}\vec{L}'}_{\mu\nu}\,\mathrm{d}^3r, \qquad (20)
\end{aligned}
$$

and the spin-magnetization part with $u \in \{x,y,z\}$ reads

$$
\begin{aligned}
V^{\mathrm{XC},\vec{L}\vec{L}'}_{\mu\nu,u} = {} & \frac{m_u}{2s}\int\left[\frac{\partial g^{\mathrm{XC}}}{\partial n_\uparrow}-\frac{\partial g^{\mathrm{XC}}}{\partial n_\downarrow}\right]\chi^{\vec{L}}_\mu(\vec{r})\,\chi^{\vec{L}'}_\nu(\vec{r})\,\mathrm{d}^3r \\
& + \frac{m_u}{2s}\int\left[\frac{|\vec{j}_\uparrow|^2}{2n_\uparrow^2}\frac{\partial g^{\mathrm{XC}}}{\partial n_\downarrow}-\frac{|\vec{j}_\downarrow|^2}{2n_\downarrow^2}\frac{\partial g^{\mathrm{XC}}}{\partial \tilde{\tau}_\downarrow}\right]\chi^{\vec{L}}_\mu(\vec{r})\,\chi^{\vec{L}'}_\nu(\vec{r})\mathrm{d}^3r \\
& - \frac{m_u}{2s}\int\left[2\frac{\partial g^{\mathrm{XC}}}{\partial \gamma_{\uparrow\uparrow}}\vec{\nabla}n_\uparrow - 2\frac{\partial g^{\mathrm{XC}}}{\partial \gamma_{\downarrow\downarrow}}\vec{\nabla}n_\downarrow - \frac{\partial g^{\mathrm{XC}}}{\partial \gamma_{\uparrow\downarrow}}(\vec{\nabla}n_\uparrow-\vec{\nabla}n_\downarrow)\right] \\
& \times\left[\left\{\vec{\nabla}\chi^{\vec{L}}_\mu(\vec{r})\right\}\chi^{\vec{L}'}_\nu(\vec{r}) + \chi^{\vec{L}}_\mu(\vec{r})\left\{\vec{\nabla}\chi^{\vec{L}'}_\nu(\vec{r})\right\}\right]\mathrm{d}^3r \\
& + \int\frac{m_u}{2s}\left[\frac{\partial g^{\mathrm{XC}}}{\partial \tilde{\tau}_\uparrow}-\frac{\partial g^{\mathrm{XC}}}{\partial \tilde{\tau}_\downarrow}\right]\left[\vec{\nabla}\chi^{\vec{L}}_\mu(\vec{r})\right]\cdot\left[\vec{\nabla}\chi^{\vec{L}'}_\nu(\vec{r})\right]\mathrm{d}^3r \\
& + \mathrm{i}\int\frac{m_u}{2s}\left[\frac{\vec{j}_\uparrow}{n_\uparrow}\frac{\partial g^{\mathrm{XC}}}{\partial \tilde{\tau}_\uparrow}-\frac{\vec{j}_\downarrow}{n_\downarrow}\frac{\partial g^{\mathrm{XC}}}{\partial \tilde{\tau}_\downarrow}\right]\xi^{\vec{L}\vec{L}'}_{\mu\nu}\,\mathrm{d}^3r. \qquad (21)
\end{aligned}
$$

The spin blocks of the Kohn–Sham equations are formed by combining the scalar and spin-magnetization contributions with the respective Pauli matrices, cf. Refs. 36 and 56. After transformation to the k space, the Kohn–Sham equations can be solved as usual.

For non-magnetic or closed-shell systems, $\vec{m}$ and $\vec{j}_\mathrm{p}$ vanish so that a Kramers-restricted framework can be applied and time-reversal symmetry[57] may be exploited. However, the spin current densities are still non-zero, and hence, the spin-up and spin-down quantities $\vec{j}_{\uparrow,\downarrow}$ contribute to the XC potential through the diamagnetic or quadratic terms.[36]

The CDFT approach outlined herein is implemented in the Riper module[56,58–64] of TURBOMOLE.[65–67] The numerical integration of the exchange–correlation potential is carried out with the algorithm outlined in Ref. 59. Note that the current density also leads to antisymmetric contributions. Integration weights are constructed according to Stratmann *et al.*[68] Geometry gradients and stress tensors are implemented based on previous work, as they essentially involve further derivatives of the basis functions.[56,61,63] Therefore, the generalization of a molecular implementation[24,36,69] to periodic systems is straightforward. We note that all integrals and the exchange potential for the Kohn–Sham equations are evaluated in the position space, which allows us to exploit sparsity. The increase in the computational cost of calculating the current density contributions on a grid is modest—especially compared to the inclusion of the current density through Hartree–Fock exchange with hybrid functions.

III. COMPUTATIONAL METHODS

First, we study the impact of the current density on the magnetic transition of one-dimensional linear Pt chains.[70–74] Two Pt atoms are placed in the unit cell, with the cell parameter d ranging

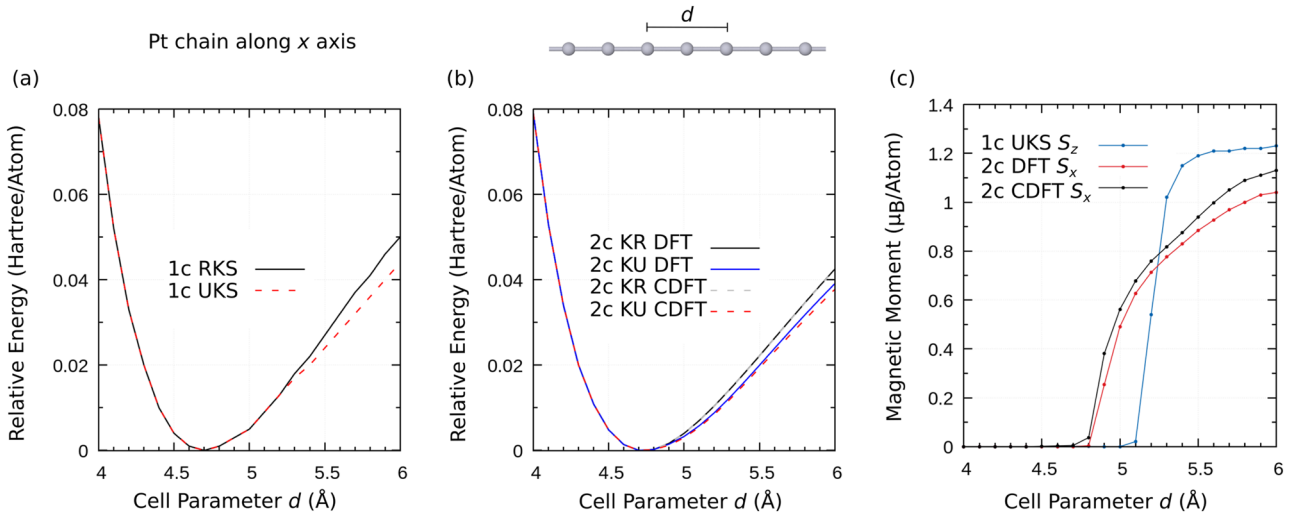

FIG. 1. (a) Dependence of the energy on the cell parameter in units of Hartree per atom for one-component (1c) restricted Kohn–Sham (RKS) and 1c unrestricted Kohn–Sham (UKS) at the TPSS/dhf-SVP-2c level. (b) Dependence of the energy on the cell parameter in units of Hartree per atom for 2c KR and 2c KU with the spin aligned along x (S_x). (c) Magnetic moment in units of Bohr's magneton μ_B per atom for the spin contribution of 1c UKS, 2c KU S_x DFT, and CDFT approaches. Periodicity is along the x direction for one-dimensional systems.[55] The open-shell solutions, are energetically favored compared to the respective closed-shell solutions and the S_x alignment is preferred over $S_{y,z}$. Results without the current-independent TPSS functional are taken from Ref. 56. Detailed results are listed in the supplementary material.

from 4.0 to 6.0 Å. Calculations are performed at the TPSS/dhf-SVP-2c[75,76] level employing Dirac–Fock effective core potentials (DF-ECPs),[77] replacing 60 electrons (ECP-60). A Gaussian smearing of 0.01 hartree[78] is used, and a *k*-mesh with 32 points is applied. Integration grids, convergence settings, etc. are given in the supplementary material. To validate the implementation with periodic boundary conditions, we carried out calculations for finite Pt chains with 2, 4, 6, 8, 10, 20, 30, 40, and 50 atoms with an interatomic distance of 3.0 Å (see the supplementary material). Here, the energy per atom converges toward the results from the periodic approach. The finite chain with 30 Pt atoms already leads to an agreement better than 0.2 millihartree, or 1 kcal/mol. We note in passing that the Karlsruhe dhf-type basis sets were optimized for discrete systems;[76] however, the corresponding pob-type basis sets for periodic calculations[79–84] are not yet available with tailored extensions for spin–orbit two-component calculations.[85] Therefore, and for consistency with previous studies, we apply the dhf-type basis sets.

Second, the band gaps and the Rashba splitting of the transition-metal dichalcogenide monolayers $MoCh_2$ and WCh_2 (Ch = S, Se, Te) in the hexagonal (2H) phase are studied with the M06-L,[86] r2SCAN,[87,88] TASK,[89] TPSS,[75] Tao–Mo,[5] and PKZB[90] functionals. The GGA PBE[91] serves as a reference. The dhf-TZVP-2c basis set[76] is applied with DF-ECPs for Mo (ECP-28), W (ECP-60), Se (ECP-10), and Te (ECP-28).[77,92,93] Structures are taken from Ref. 94. A *k*-mesh of 33 × 33 points is applied.

Third, the CDFT framework is applied to complement our previous meta-GGA study on silver halides.[56] Here, we consider the TPSS,[75] revTPSS,[95,96] Tao–Mo,[5] PKZB,[90] r^{2}SCAN,[87,88] and M06-L.[86] We use the dhf-SVP basis set,[76] and DF-ECPs are applied for Ag (ECP-28) and I (ECP-28).[97,98] A *k*-mesh of 7 × 7 × 7 is employed.

IV. RESULTS AND DISCUSSION

A. Linear Pt chain

The one-dimensional linear Pt chain is a common reference system for a transition to a magnetic system. The closed-shell configuration constitutes the electronic ground state with a small cell parameter, whereas the magnetic open-shell solution becomes lower in energy with increasing cell size.[70–74] This is also confirmed at the scalar and spin–orbit TPSS levels in Fig. 1. For small cell parameters

TABLE I. Band gaps and Rashba splittings of the valence band at the K point for transition-metal dichalcogenide monolayers at the 1c DFT, 2c DFT, and 2c CDFT levels with the dhf-TZVP-2c basis set and DF-ECPs for all atoms. All values are in eV. Results for MoS_2 and WS_2 are listed in the supplementary material.

		Band gap			Rashba splitting	
System	DFA	1c DFT	2c DFT	2c CDFT	2c DFT	2c CDFT
$MoSe_2$	PBE	1.554	1.453	⋯	0.166	⋯
	PKZB	1.558	1.455	1.455	0.166	0.169
	Tao–Mo	1.561	1.459	1.458	0.166	0.170
	TPSS	1.563	1.459	1.458	0.167	0.174
	M06-L	1.563	1.460	1.455	0.170	0.181
	r^{2}SCAN	1.657	1.554	1.544	0.166	0.189
	TASK	1.735	1.629	1.607	0.172	0.218
$MoTe_2$	PBE	1.157	1.039	⋯	0.185	⋯
	PKZB	1.160	1.042	1.042	0.186	0.189
	Tao–Mo	1.168	1.051	1.049	0.185	0.188
	TPSS	1.170	1.051	1.048	0.185	0.195
	M06-L	1.182	1.060	1.053	0.192	0.209
	r^{2}SCAN	1.235	1.116	1.101	0.186	0.218
	TASK	1.287	1.161	1.126	0.197	0.269
WSe_2	PBE	1.627	1.324	⋯	0.409	⋯
	PKZB	1.652	1.377	1.374	0.407	0.410
	Tao–Mo	1.667	1.371	1.367	0.403	0.411
	TPSS	1.660	1.379	1.371	0.409	0.420
	M06-L	1.668	1.413	1.405	0.422	0.440
	r^{2}SCAN	1.774	1.482	1.452	0.419	0.457
	TASK	1.867	1.604	1.571	0.440	0.514
WTe_2	PBE	1.219	0.933	⋯	0.423	⋯
	PKZB	1.227	0.953	0.951	0.423	0.427
	Tao–Mo	1.241	0.963	0.957	0.419	0.426
	TPSS	1.237	0.960	0.954	0.422	0.435
	M06-L	1.253	0.968	0.957	0.431	0.456
	r^{2}SCAN	1.325	1.039	1.005	0.436	0.483
	TASK	1.388	1.096	1.050	0.465	0.566

from $d = 4.0$ to 4.8 Å, the open-shell initial guess generally converges to a closed-shell non-magnetic solution in the self-consistent field (SCF) procedure. The most favorable total energy is found for $d = 4.7$ Å, in agreement with previous studies based on GGA functionals.[56,73] Furthermore, CDFT and DFT lead to a very similar potential energy surface or a similar behavior of the relative energy with respect to the cell parameter d.

At the scalar level, the transition to a magnetic material occurs at around $d \approx 5.2$ Å. The inclusion of spin–orbit coupling shifts this transition to a smaller d parameter of about 4.9 Å. For CDFT, a small magnetic moment is already found at 4.8 Å. Here, the current-dependent variant of TPSS (cTPSS) leads to a lower total energy for both closed-shell and open-shell solutions, i.e., a more negative energy and a larger magnetic moment. The impact of the current density is generally greater for the magnetic solution than for the closed-shell state; see also the supplementary material for detailed results. For the closed-shell solution, the difference in total energy by the inclusion of the current density is too small to be visible in panel (b) of Fig. 1. This finding is qualitatively in line with our previous studies on molecular systems.[36]

The inclusion of the current density also consistently leads to a larger magnetic moment. For instance, TPSS predicts a magnetic moment of 1.04 μ_B/atom at $d = 6.0$ Å, whereas a value of 1.13 μ_B/atom is found with cTPSS. Generally, an increase in the range of 5–8% is observed after the transition to a magnetic solution.

B. Transition-metal dichalcogenide monolayers

Transition-metal dichalcogenide monolayers have many interesting physical properties, such as the quantum spin Hall,[99] non-linear anomalous Hall,[100] and Rashba effects.[101] In the H2 phase, time-reversal symmetry holds for the non-magnetic systems, but space-inversion symmetry is lost. Thus, spin–orbit coupling lifts the degeneracy of the valence band at the K point in the Brillouin zone. For the Mo and W systems, this Rashba splitting is very pronounced, and values between 0.1 and 0.5 eV are obtained with relativistic all-electron methods.[94,102]

Band gaps and Rashba splittings at the K point obtained with DFT and CDFT approaches are listed in Table I. On the one hand, the impact on the band gaps is rather small, with TASK and r^{2}SCAN showing the largest changes but not exceeding 0.1 eV. Here, the deviation between the different DFAs is far larger. On the other hand, Rashba splitting is very sensitive to the inclusion of the current density. For instance, the results change from 0.436 to 0.483 eV and 0.465–0.566 eV for WTe_2 with r^{2}SCAN and TASK, respectively.

The most pronounced current-density effects are found for TASK throughout all systems, which is in line with molecular studies.[36,53,103] Here, the current density increases the Rashba splitting by 25% on average. r^{2}SCAN ranks second in this regard with 13%, followed by M06-L with 6%. For PKZB, Tao–Mo, and TPSS, changes of only 1–3% are observed. Among the different monolayers, $MoTe_2$ leads to the largest impact of the current density for all DFAs, with a relative deviation of 36% between DFT and CDFT for TASK. The impact of the current density on the DFAs can be rationalized by the enhancement factor.[103,104]

C. Silver halide crystals

The band gaps and optimized lattice constants of AgI with various meta-GGAs are listed in Table II. Results for AgCl and AgBr are

TABLE II. Optimized lattice constant a (in Å, rocksalt structure) of three-dimensional AgI and band gaps (in eV) at high symmetry points of the first Brillouin zone with various density functional approximations and the dhf-SVP basis sets. A "c" indicates the current-dependent variant of the DFA. Results for DFAs without the inclusion of the current density are taken from Ref. 56, except for M06-L. Calculations are performed without dispersion correction (no D3) and with the D3 correction using Becke–Johnson damping (D3-BJ).

DFA	Dispersion	a	L–L	Γ–Γ	X–X	L–X
TPSS	no D3	6.153	3.249	2.047	2.937	0.583
cTPSS	no D3	6.150	3.244	2.052	2.940	0.579
revTPSS	no D3	6.116	3.149	2.132	2.998	0.537
crevTPSS	no D3	6.098	3.122	2.161	3.014	0.512
Tao–Mo	no D3	6.071	3.099	2.343	3.108	0.616
cTao–Mo	no D3	6.069	3.086	2.339	3.109	0.619
PKZB	no D3	6.200	3.409	2.153	2.987	0.826
cPKZB	no D3	6.210	3.422	2.138	2.979	0.839
r^{2}SCAN	no D3	6.159	3.776	2.501	3.237	0.911
cr^{2}SCAN	no D3	6.156	3.772	2.504	3.240	0.907
M06-L	no D3	6.325	3.511	1.891	2.976	1.116
cM06-L	no D3	6.327	3.512	1.889	2.974	1.117
TPSS	D3-BJ	5.982	2.988	2.352	3.098	0.343
cTPSS	D3-BJ	5.980	2.985	2.354	3.099	0.341
revTPSS	D3-BJ	5.949	2.883	2.443	3.156	0.291
crevTPSS	D3-BJ	5.952	2.889	2.435	3.152	0.296
Tao–Mo	D3-BJ	6.068	3.095	2.347	3.110	0.613
cTao–Mo	D3-BJ	6.062	3.087	2.358	3.116	0.604
r^{2}SCAN	D3-BJ	6.156	3.773	2.506	3.240	0.907
cr^{2}SCAN	D3-BJ	6.155	3.771	2.506	3.241	0.905

presented in the supplementary material. Overall, the current density is of minor importance for the band gaps. Changes are in the order of meV. These results are in qualitative agreement with the two-dimensional $MoTe_2$ monolayer, which consists of atoms from the same row of the periodic table of elements.

Similarly, the current density does not lead to major changes for the cell structure or the lattice constant. The small impact on the lattice constant can be rationalized by the comparably small impact of spin–orbit coupling on the cell structure.[56] D3 dispersion correction with Becke–Johnson damping[8,105–108] (D3-BJ) leads to much larger changes than the application of CDFT. Therefore, other computational parameters than the inclusion of the current density for meta-GGAs are more important for the cell structures of the silver halide crystals.

V. CONCLUSION

We have extended our previous formulation of spin–orbit current density functional theory to periodic systems of arbitrary dimension. The impact of the current density was assessed for various properties of non-magnetic and magnetic systems. Here, the band gaps and lattice constants are not notably affected. In contrast, the Rashba splitting, which is only due to spin–orbit coupling, is substantially affected. The inclusion of the current density for a given functional may lead to larger changes than the deviation of the results among different functionals.

With the present work, CDFT is now applicable to a wide range of chemical and physical properties of discrete and periodic systems, including analytic first-order property calculations. We generally recommend including the current density for r^2SCAN and the Minnesota functionals, if available, in the used electronic structure code. For TASK, the inclusion of the current density is clearly mandatory as it leads to substantial changes in the results.

SUPPLEMENTARY MATERIAL

The supplementary material is available with all computational details and data.

ACKNOWLEDGMENTS

We thank Fabian Pauly (Augsburg) and Marek Sierka (Jena) for their helpful comments. Y.J.F. gratefully acknowledges the support via the Walter–Benjamin program funded by the Deutsche Forschungsgemeinschaft (DFG, German Research Foundation)—Grant No. 518707327. C.H. gratefully acknowledges the funding from the Volkswagen Foundation.

AUTHOR DECLARATIONS

Conflict of Interest

The authors have no conflicts to disclose.

Author Contributions

Yannick J. Franzke: Conceptualization (equal); Data curation (lead); Formal analysis (lead); Investigation (equal); Methodology (lead); Software (lead); Validation (equal); Visualization (lead); Writing – original draft (lead); Writing – review & editing (equal). **Christof Holzer**: Conceptualization (equal); Data curation (supporting); Formal analysis (supporting); Investigation (equal); Methodology (supporting); Software (supporting); Validation (equal); Writing – original draft (supporting); Writing – review & editing (equal).

DATA AVAILABILITY

The data that support the findings of this study are available within the article and its supplementary material.

REFERENCES

[1] K. Burke, J. Chem. Phys. **136**, 150901 (2012).
[2] A. D. Becke, J. Chem. Phys. **140**, 18A301 (2014).
[3] J. Sun, A. Ruzsinszky, and J. P. Perdew, Phys. Rev. Lett. **115**, 036402 (2015).
[4] N. Mardirossian and M. Head-Gordon, Mol. Phys. **115**, 2315 (2017).
[5] J. Tao and Y. Mo, Phys. Rev. Lett. **117**, 073001 (2016).
[6] P. Hao, J. Sun, B. Xiao, A. Ruzsinszky, G. I. Csonka, J. Tao, S. Glindmeyer, and J. P. Perdew, J. Chem. Theory Comput. **9**, 355 (2013).
[7] Y. Mo, R. Car, V. N. Staroverov, G. E. Scuseria, and J. Tao, Phys. Rev. B **95**, 035118 (2017).
[8] L. Goerigk, A. Hansen, C. Bauer, S. Ehrlich, A. Najibi, and S. Grimme, Phys. Chem. Chem. Phys. **19**, 32184 (2017).
[9] Y. J. Franzke and J. M. Yu, J. Chem. Theory Comput. **18**, 323 (2022).
[10] Y. J. Franzke and J. M. Yu, J. Chem. Theory Comput. **18**, 2246 (2022).
[11] A. D. Becke, J. Chem. Phys. **156**, 214101 (2022).
[12] P. Borlido, T. Aull, A. W. Huran, F. Tran, M. A. L. Marques, and S. Botti, J. Chem. Theory Comput. **15**, 5069 (2019).
[13] C. Holzer, Y. J. Franzke, and M. Kehry, J. Chem. Theory Comput. **17**, 2928 (2021).
[14] M. Kehry, Y. J. Franzke, C. Holzer, and W. Klopper, Mol. Phys. **118**, e1755064 (2020).
[15] J. Lee, X. Feng, L. A. Cunha, J. F. Gonthier, E. Epifanovsky, and M. Head-Gordon, J. Chem. Phys. **155**, 164102 (2021).
[16] A. Ghosh, S. Jana, T. Rauch, F. Tran, M. A. L. Marques, S. Botti, L. A. Constantin, M. K. Niranjan, and P. Samal, J. Chem. Phys. **157**, 124108 (2022).
[17] P. Kovás, F. Tran, P. Blaha, and G. K. H. Madsen, J. Chem. Phys. **157**, 094110 (2022).
[18] J. Liang, X. Feng, D. Hait, and M. Head-Gordon, J. Chem. Theory Comput. **18**, 3460 (2022).
[19] Y. J. Franzke, J. Chem. Theory Comput. **19**, 2010 (2023).
[20] P. Kovács, P. Blaha, and G. K. H. Madsen, J. Chem. Phys. **159**, 244118 (2023).
[21] T. Lebeda, T. Aschebrock, J. Sun, L. Leppert, and S. Kümmel, Phys. Rev. Mater. **7**, 093803 (2023).
[22] J. W. Furness, J. Verbeke, E. I. Tellgren, S. Stopkowicz, U. Ekström, T. Helgaker, and A. M. Teale, J. Chem. Theory Comput. **11**, 4169 (2015).
[23] E. I. Tellgren, A. M. Teale, J. W. Furness, K. K. Lange, U. Ekström, and T. Helgaker, J. Chem. Phys. **140**, 034101 (2014).
[24] T. J. P. Irons, G. David, and A. M. Teale, J. Chem. Theory Comput. **17**, 2166 (2021).
[25] A. Pausch and C. Holzer, J. Phys. Chem. Lett. **13**, 4335 (2022).
[26] T. Saue, "Spin-interactions and the non-relativistic limit of electrodynamics," in *Advances in Quantum Chemistry, Vol. 48*, edited by J. R. Sabin, E. Brändas, and L. B. Oddershede (Elsevier Academic Press, San Diego, CA, 2005), pp. 383–405.
[27] T. Saue, ChemPhysChem **12**, 3077 (2011).
[28] P. Pyykkö, Annu. Rev. Phys. Chem. **63**, 45 (2012).
[29] J. F. Dobson, J. Chem. Phys. **98**, 8870 (1993).
[30] J. Tao, Phys. Rev. B **71**, 205107 (2005).
[31] S. Pittalis, S. Kurth, S. Sharma, and E. K. U. Gross, J. Chem. Phys. **127**, 124103 (2007).

[32]E. Räsänen, S. Pittalis, and C. R. Proetto, J. Chem. Phys. **132**, 044112 (2010).
[33]S. Pittalis, E. Räsänen, and E. K. U. Gross, Phys. Rev. A **80**, 032515 (2009).
[34]J. E. Bates and F. Furche, J. Chem. Phys. **137**, 164105 (2012).
[35]T. M. Maier, Y. Ikabata, and H. Nakai, J. Chem. Phys. **152**, 214103 (2020).
[36]C. Holzer, Y. J. Franzke, and A. Pausch, J. Chem. Phys. **157**, 204102 (2022).
[37]J. K. Desmarais, G. Ambrogio, G. Vignale, A. Erba, and S. Pittalis, Phys. Rev. Mater. **8**, 013802 (2024).
[38]J. K. Desmarais, J. Maul, B. Civalleri, A. Erba, G. Vignale, and S. Pittalis, arXiv:2401.07581 (2024).
[39]E. I. Tellgren, S. Kvaal, E. Sagvolden, U. Ekström, A. M. Teale, and T. Helgaker, Phys. Rev. A **86**, 062506 (2012).
[40]A. D. Becke, J. Chem. Phys. **117**, 6935 (2002).
[41]J. Kübler, K.-H. Höck, J. Sticht, and A. R. Williams, J. Phys. F: Met. Phys. **18**, 469 (1988).
[42]C. Van Wüllen, J. Comput. Chem. **23**, 779 (2002).
[43]T. Saue and T. Helgaker, J. Comput. Chem. **23**, 814 (2002).
[44]M. K. Armbruster, F. Weigend, C. van Wüllen, and W. Klopper, Phys. Chem. Chem. Phys. **10**, 1748 (2008).
[45]J. E. Peralta, G. E. Scuseria, and M. J. Frisch, Phys. Rev. B **75**, 125119 (2007).
[46]G. Scalmani and M. J. Frisch, J. Chem. Theory Comput. **8**, 2193 (2012).
[47]I. W. Bulik, G. Scalmani, M. J. Frisch, and G. E. Scuseria, Phys. Rev. B **87**, 035117 (2013).
[48]A. Baldes and F. Weigend, Mol. Phys. **111**, 2617 (2013).
[49]F. Egidi, S. Sun, J. J. Goings, G. Scalmani, M. J. Frisch, and X. Li, J. Chem. Theory Comput. **13**, 2591 (2017).
[50]S. Komorovsky, P. J. Cherry, and M. Repisky, J. Chem. Phys. **151**, 184111 (2019).
[51]J. K. Desmarais, S. Komorovsky, J.-P. Flament, and A. Erba, J. Chem. Phys. **154**, 204110 (2021).
[52]F. Bruder, Y. J. Franzke, and F. Weigend, J. Phys. Chem. A **126**, 5050 (2022).
[53]F. Bruder, Y. J. Franzke, C. Holzer, and F. Weigend, J. Chem. Phys. **159**, 194117 (2023).
[54]Y. J. Franzke, F. Bruder, S. Gillhuber, C. Holzer, and F. Weigend, J. Phys. Chem. A **128**, 670 (2024).
[55]TURBOMOLE GmbH, Manual of TURBOMOLE V7.8.1, a development of University of Karlsruhe and Forschungszentrum Karlsruhe GmbH, 1989–2007, TURBOMOLE GmbH, since 2007; available at https://www.turbomole.org/turbomole/turbomole-documentation/ (retrieved March 4, 2024).
[56]Y. J. Franzke, W. M. Schosser, and F. Pauly, Phys. Rev. B **109**, 165144 (2024).
[57]J. M. Kasper, A. J. Jenkins, S. Sun, and X. Li, J. Chem. Phys. **153**, 090903 (2020).
[58]A. M. Burow, M. Sierka, and F. Mohamed, J. Chem. Phys. **131**, 214101 (2009).
[59]A. M. Burow and M. Sierka, J. Chem. Theory Comput. **7**, 3097 (2011).
[60]R. Łazarski, A. M. Burow, and M. Sierka, J. Chem. Theory Comput. **11**, 3029 (2015).
[61]R. Łazarski, A. M. Burow, L. Grajciar, and M. Sierka, J. Comput. Chem. **37**, 2518 (2016).
[62]L. Grajciar, J. Comput. Chem. **36**, 1521 (2015).
[63]M. Becker and M. Sierka, J. Comput. Chem. **40**, 2563 (2019).
[64]A. Irmler, A. M. Burow, and F. Pauly, J. Chem. Theory Comput. **14**, 4567 (2018).
[65]R. Ahlrichs, M. Bär, M. Häser, H. Horn, and C. Kölmel, Chem. Phys. Lett. **162**, 165 (1989).
[66]Y. J. Franzke, C. Holzer, J. H. Andersen, T. Begušić, F. Bruder, S. Coriani, F. Della Sala, E. Fabiano, D. A. Fedotov, S. Fürst, S. Gillhuber, R. Grotjahn, M. Kaupp, M. Kehry, M. Krstić, F. Mack, S. Majumdar, B. D. Nguyen, S. M. Parker, F. Pauly, A. Pausch, E. Perlt, G. S. Phun, A. Rajabi, D. Rappoport, B. Samal, T. Schrader, M. Sharma, E. Tapavicza, R. S. Treß, V. Voora, A. Wodyński, J. M. Yu, B. Zerulla, F. Furche, C. Hättig, M. Sierka, D. P. Tew, and F. Weigend, J. Chem. Theory Comput. **19**, 6859 (2023).
[67]TURBOMOLE GmbH, Developers' version of TURBOMOLE V7.8.1, a development of University of Karlsruhe and Forschungszentrum Karlsruhe GmbH, 1989–2007, TURBOMOLE GmbH, since 2007; available at https://www.turbomole.org (retrieved March 4, 2024).
[68]R. Stratmann, G. E. Scuseria, and M. J. Frisch, Chem. Phys. Lett. **257**, 213 (1996).
[69]A. I. Pausch, "Development and application of efficient computational methods for molecular spectroscopy in finite magnetic fields," Dissertation (Dr. rer. nat.), Karlsruhe Institute of Technology (KIT), Germany, 2022.
[70]A. Delin and E. Tosatti, Phys. Rev. B **68**, 144434 (2003).
[71]A. Delin and E. Tosatti, Surf. Sci. **566–568**, 262 (2004).
[72]J. Fernández-Rossier, D. Jacob, C. Untiedt, and J. J. Palacios, Phys. Rev. B **72**, 224418 (2005).
[73]A. Smogunov, A. Dal Corso, A. Delin, R. Weht, and E. Tosatti, Nat. Nanotechnol. **3**, 22 (2008).
[74]V. M. García-Suárez, D. Z. Manrique, C. J. Lambert, and J. Ferrer, Phys. Rev. B **79**, 060408(R) (2009).
[75]J. Tao, J. P. Perdew, V. N. Staroverov, and G. E. Scuseria, Phys. Rev. Lett. **91**, 146401 (2003).
[76]F. Weigend and A. Baldes, J. Chem. Phys. **133**, 174102 (2010).
[77]D. Figgen, K. A. Peterson, M. Dolg, and H. Stoll, J. Chem. Phys. **130**, 164108 (2009).
[78]G. Kresse and J. Furthmüller, Comput. Mater. Sci. **6**, 15 (1996).
[79]M. F. Peintinger, D. V. Oliveira, and T. Bredow, J. Comput. Chem. **34**, 451 (2013).
[80]J. Laun, D. Vilela Oliveira, and T. Bredow, J. Comput. Chem. **39**, 1285 (2018).
[81]D. Vilela Oliveira, J. Laun, M. F. Peintinger, and T. Bredow, J. Comput. Chem. **40**, 2364 (2019).
[82]J. Laun and T. Bredow, J. Comput. Chem. **42**, 1064 (2021).
[83]J. Laun and T. Bredow, J. Comput. Chem. **43**, 839 (2022).
[84]L. M. Seidler, J. Laun, and T. Bredow, J. Comput. Chem. **44**, 1418 (2023).
[85]M. K. Armbruster, W. Klopper, and F. Weigend, Phys. Chem. Chem. Phys. **8**, 4862 (2006).
[86]Y. Zhao and D. G. Truhlar, J. Chem. Phys. **125**, 194101 (2006).
[87]J. W. Furness, A. D. Kaplan, J. Ning, J. P. Perdew, and J. Sun, J. Phys. Chem. Lett. **11**, 8208 (2020).
[88]J. W. Furness, A. D. Kaplan, J. Ning, J. P. Perdew, and J. Sun, J. Phys. Chem. Lett. **11**, 9248 (2020).
[89]T. Aschebrock and S. Kümmel, Phys. Rev. Res. **1**, 033082 (2019).
[90]J. P. Perdew, S. Kurth, A. c. v. Zupan, and P. Blaha, Phys. Rev. Lett. **82**, 2544 (1999).
[91]J. P. Perdew, K. Burke, and M. Ernzerhof, Phys. Rev. Lett. **77**, 3865 (1996).
[92]K. A. Peterson, D. Figgen, E. Goll, H. Stoll, and M. Dolg, J. Chem. Phys. **119**, 11113 (2003).
[93]K. A. Peterson, D. Figgen, M. Dolg, and H. Stoll, J. Chem. Phys. **126**, 124101 (2007).
[94]P. Miró, M. Audiffred, and T. Heine, Chem. Soc. Rev. **43**, 6537 (2014).
[95]J. P. Perdew, A. Ruzsinszky, G. I. Csonka, L. A. Constantin, and J. Sun, Phys. Rev. Lett. **103**, 026403 (2009).
[96]J. P. Perdew, A. Ruzsinszky, G. I. Csonka, L. A. Constantin, and J. Sun, Phys. Rev. Lett. **106**, 179902 (2011).
[97]D. Figgen, G. Rauhut, M. Dolg, and H. Stoll, Chem. Phys. **311**, 227 (2005).
[98]K. A. Peterson, B. C. Shepler, D. Figgen, and H. Stoll, J. Phys. Chem. A **110**, 13877 (2006).
[99]C.-C. Liu, W. Feng, and Y. Yao, Phys. Rev. Lett. **107**, 076802 (2011).
[100]K. Kang, T. Li, E. Sohn, J. Shan, and K. F. Mak, Nat. Mater. **18**, 324 (2019).
[101]Z. Y. Zhu, Y. C. Cheng, and U. Schwingenschlögl, Phys. Rev. B **84**, 153402 (2011).
[102]M. Kadek, B. Wang, M. Joosten, W.-C. Chiu, F. Mairesse, M. Repisky, K. Ruud, and A. Bansil, Phys. Rev. Mater. **7**, 064001 (2023).
[103]Y. J. Franzke and C. Holzer, J. Chem. Phys. **157**, 031102 (2022).
[104]R. Grotjahn, F. Furche, and M. Kaupp, J. Chem. Phys. **157**, 111102 (2022).
[105]S. Grimme, J. Antony, S. Ehrlich, and H. Krieg, J. Chem. Phys. **132**, 154104 (2010).
[106]S. Grimme, S. Ehrlich, and L. Goerigk, J. Comput. Chem. **32**, 1456 (2011).
[107]A. Patra, S. Jana, L. A. Constantin, and P. Samal, J. Chem. Phys. **153**, 084117 (2020).
[108]S. Ehlert, U. Huniar, J. Ning, J. W. Furness, J. Sun, A. D. Kaplan, J. P. Perdew, and J. G. Brandenburg, J. Chem. Phys. **154**, 061101 (2021).